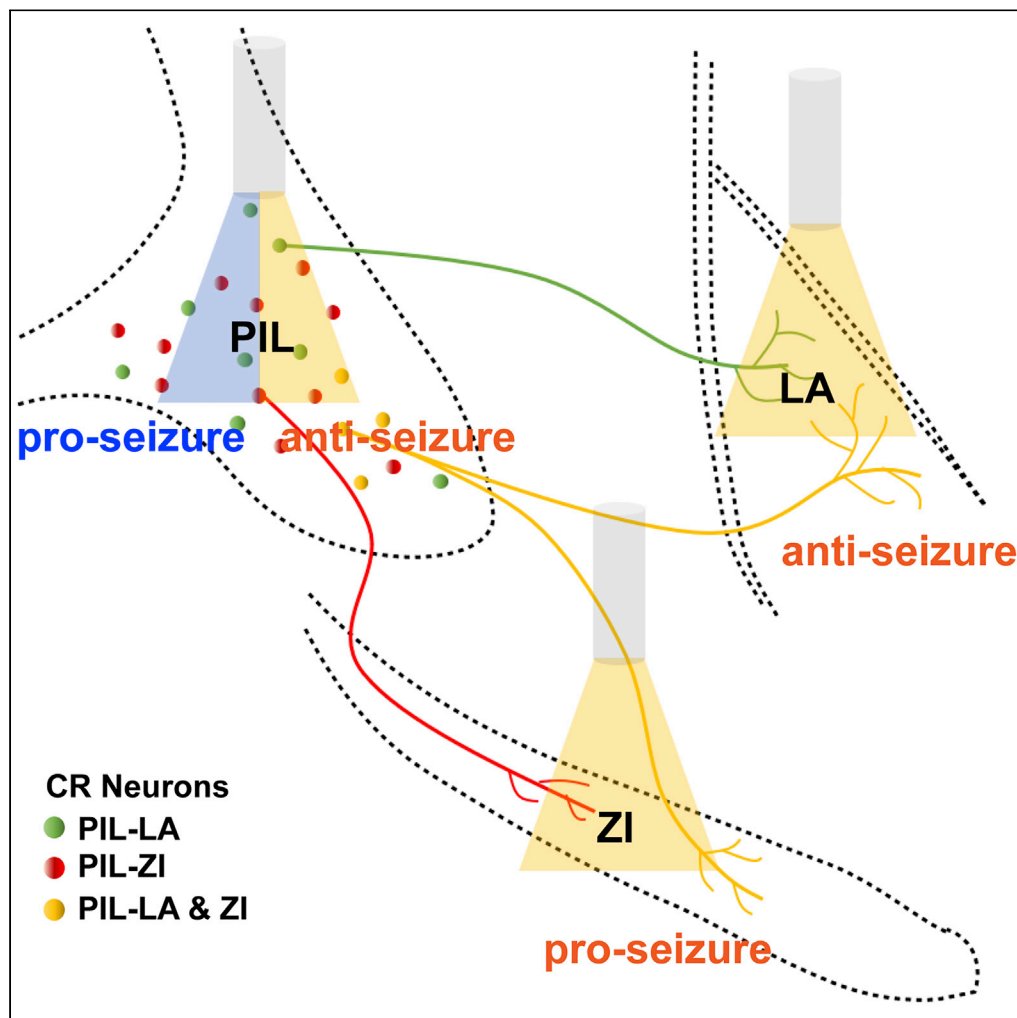# iScience

Article

Paradoxical effects of posterior intralaminar thalamic calretinin neurons on hippocampal seizure via distinct downstream circuits

Yingbei Qi,
Heming Cheng,
Qiuwen Lou, ...,
Yeping Ruan,
Zhong Chen, Yi
Wang

chenzhong@zju.edu.cn (Z.C.)
wang-yi@zju.edu.cn (Y.W.)

Highlights

PIL CR neurons are
activated during
hippocampal seizures

Optogenetic control of
PIL CR neurons
bidirectionally modulates
seizure development

LA-projecting and ZI-
projecting CR circuits
present opposite effects
in seizure modulation

iScience

Article

Paradoxical effects of posterior intralaminar thalamic calretinin neurons on hippocampal seizure via distinct downstream circuits

Yingbei Qi,[1,4] Heming Cheng,[2,4] Qiuwen Lou,[2] Xia Wang,[1] Nanxi Lai,[1] Chenshu Gao,[2] Shuangshuang Wu,[2] Cenglin Xu,[2] Yeping Ruan,[2] Zhong Chen,[1,2,3,5,*] and Yi Wang[1,2,3,5,*]

SUMMARY

Epilepsy is a circuit-level brain disorder characterized by hyperexcitatory seizures with unclear mechanisms. Here, we investigated the causal roles of calretinin (CR) neurons in the posterior intralaminar thalamic nucleus (PIL) in hippocampal seizures. Using c-fos mapping and calcium fiber photometry, we found that PIL CR neurons were activated during hippocampal seizures in a kindling model. Optogenetic activation of PIL CR neurons accelerated seizure development, whereas inhibition retarded seizure development. Further, viral-based circuit tracing verified that PIL CR neurons were long-range glutamatergic neurons, projecting toward various downstream regions. Interestingly, selective inhibition of PIL-lateral amygdala CR circuit attenuated seizure progression, whereas inhibition of PIL-zona incerta CR circuit presented an opposite effect. These results indicated that CR neurons in the PIL play separate roles in hippocampal seizures via distinct downstream circuits, which complements the pathogenic mechanisms of epilepsy and provides new insight for the precise medicine of epilepsy.

INTRODUCTION

Temporal lobe epilepsy (TLE) is one of the most common types of human epilepsy and can often develop into refractory epilepsy, bringing heavy physiological and psychological burdens to the patients and their family (Bialer and White, 2010; Fialho et al., 2018; Lin et al., 2012; Xu et al., 2016). Current treatments including antiepileptic drugs and surgery can only partially control seizure and may often induce adverse effects, which could be associated with the unrevealing pathogenetic mechanisms of epilepsy (Fiest et al., 2013; Liu et al., 2017; Loscher et al., 2020; Stephen et al., 2017; Wang and Chen, 2019). As emerging studies suggest that epilepsy is associated with the dysfunction of excitatory and inhibitory circuits (Cheng et al., 2020; Wang et al., 2014, 2016, 2017, 2020), it is crucial to map out the vital circuitries and understand their functions in epilepsy.

Calretinin (CR) neuron is a type of important but heterogeneous neuron in the brain, implicated in many physiological functions including neural development, memory formation, and motor control (Barsy et al., 2020; Fonseca et al., 1995; Qi et al., 2021; Schiffmann et al., 1999). They possess different types of morphologies, release various neurotransmitters, show diverse distributions, and are also closely implicated in regulating neural and circuit excitability (Gonchar and Burkhalter, 2003; Pfeffer et al., 2013; Saffari et al., 2019). Prior studies of CR neurons in epilepsy are sparse. CR neurons in various regions, including the hippocampus, thalamus, and amygdala, showed vulnerability in both human epilepsy and animal models of epilepsy (Blumcke et al., 1999; Buckmaster et al., 2017; Drexel et al., 2011; Toth et al., 2010; Zhang et al., 2009); however, contradictions of increased number of CR neurons in some regions were also reported (Blumcke et al., 1999; Thom et al., 2002). These studies suggested that CR neurons are closely associated with seizure progression (Toth et al., 2010; Toth and Magloczky, 2014), but the causal role of CR neurons in epilepsy are still unknown because of lack of specific intervention approach. In the present study, using c-fos mapping in whole brain level and calcium fiber photometry in mouse epilepsy model, we screened out a large amount of hyperactivated CR neurons in the posterior intralaminar thalamic nucleus (PIL)—a region that contains dense CR neurons—which connects to various brain regions that are involved in epilepsy, such as the secondary auditory cortex, zona incerta (ZI), and lateral amygdala (LA) (Benini and Avoli, 2006; Franzini et al., 2008; Kita et al., 2016; Linke, 1999; Xu et al., 2021). In addition, through selective

[1]Institute of Pharmacology and Toxicology, College of Pharmaceutical Sciences, Zhejiang University, Hangzhou, China

[2]Key Laboratory of Neuropharmacology and Translational Medicine of Zhejiang Province, School of Pharmaceutical Sciences, Zhejiang Chinese Medical University, Hangzhou, China

[3]Epilepsy Center, Department of Neurology, Second Affiliated Hospital, School of Medicine, Zhejiang University, Hangzhou, China

[4]These authors contributed equally

[5]Lead contact

*Correspondence: chenzhong@zju.edu.cn (Z.C.), wang-yi@zju.edu.cn (Y.W.)

https://doi.org/10.1016/j.isci.2022.104218

modulation of the CR neurons in the PIL by optogenetics, we demonstrated the diverse roles of PIL CR neurons in epilepsy via their distinct downstream neural circuits. This may be beneficial for the precise treatment of epilepsy at a circuit level.

RESULTS

Calretinin neurons in the PIL are activated during hippocampal seizures

To map the number and activity of CR neurons in different brain regions after epileptic seizure, we immunolabeled for CR and c-Fos in mice, 1.5 h after the last generalized seizure (GS) of hippocampal kindling model—a common epilepsy model mimicking clinical focal seizure (FS) with secondary GS. Of the 38 brain regions that were tallied between sham and kindled mice, no significant changes to the amount of CR neurons were found (Figure S1A). However, there was a ~20% increase of c-Fos$^+$ CR neurons in 9 out of the 38 brain regions (Figure S1B). Among them, the PIL showed both dense CR immunoactivity (138.03 ± 36.53 cells/section in Sham, 115.91 ± 42.83 cells in kindled, Figure S1A) and a significant increase in c-Fos expression in CR neurons after GS (0% colocalization in Sham, $19.79\% \pm 8.53\%$ colocalization in kindled, Figures 1A and 1B). To directly monitor the activity of CR neurons in real time in the PIL during hippocampal seizure, *CR-cre* mice were injected with an AAV-encoded Ca^{2+} indicator GCaMP6s (*AAV2/9-Ef1a-DIO-GCaMP6s*) into the PIL (Figure 1C). The GCaMP6s virus was allowed to express for 3 weeks before surgical implantation of an optic fiber in the PIL for fiber photometry recording and electrodes in CA3 for kindling stimulation. After a 1 week recovery, we monitored Ca^{2+} activity during kindling-induced seizures. During initial FS, there is only a slight increment in Ca^{2+} activity of PIL CR neurons (Figures 1D–1G). During GS, Ca^{2+} activity of PIL CR neurons began to increase during the latency to GS and further increased to the largest degree during GS onset (Figures 1H–1K), which is consistent with the results of c-Fos data. Thus, the aforementioned results signify that the PIL CR neurons are activated during GS.

Selective activation of CR neurons in the PIL promotes seizure progression

To assess the causal role of PIL CR neurons in seizures, we used optogenetics to selectively activate PIL CR neurons in hippocampal kindling models. A cre recombinase-dependent excitatory opsin, Channelrhodopsin (ChR2, *AAV2/9-EF1α-DIO-hChR2(H134R)-eYFP*), was expressed in the PIL of *CR-cre* mice followed by a surgical procedure implanting the optic fiber and electrodes into the PIL and CA3 regions, respectively (Figure 2A). To ensure the specificity of the virus, the section of the PIL was immunostained with CR; it was found that about $80.50 \pm 2.50\%$ of eYFP$^+$ neurons were co-labeled with CR, whereas about $50.46 \pm 2.35\%$ total CR neurons expressed ChR2-eYFP (Figures 2B and 2C). Mice were delivered with yellow light (as control) or blue light into the PIL immediately after kindling stimulation. To exclude the possibility that the color of light would affect seizure susceptibility, we also set up another control group; i.e., the *CR-cre* mice were injected with *AAV2/9-EF1α-DIO-eYFP* and received blue light stimulation. We found that activating the CR neurons in the PIL significantly accelerated seizure development (Figure 2D) and increased the afterdischarge duration (ADD, Figure 2E) during kindling-induced seizure acquisition. Activation of PIL CR neurons significantly reduced the number of stimulations required to stay at stages 0-2 and 3-4; the overall number of stimulations required to achieve first GS (stage 4) was also decreased (Figures 2F and 2G). EEG and spectrum analysis demonstrated that mice given blue light showed a drastic increase in seizure intensity compared to mice given yellow light (Figures 2H and 2I). This implies that activation of PIL CR neurons promotes seizure propagation.

Selective inhibition of CR neurons in the PIL retards seizure progression

Next, we aimed to investigate whether inhibiting PIL CR neurons would have an effect on hippocampal seizures. A cre recombinase-dependent inhibitory opsin, archaerhodopsin (*AAV2/9-CAG-FLEX-ArchT-GFP*), was expressed in the PIL of *CR-cre* mice followed by a surgical procedure implanting the optic fiber and electrodes into the PIL and CA3, respectively (Figure 3A). After immunostaining with CR, we found that about $89.00 \pm 2.08\%$ of GFP$^+$ neurons were co-labeled with CR, whereas about $69.74 \pm 3.23\%$ total CR neurons expressed ArchT-GFP (Figures 3B and 3C). After recovery, mice were delivered with blue light (as control) or yellow light into the PIL immediately after kindling stimulation. To exclude the possibility that the color of light would affect seizure susceptibility, we also set up another control group; i.e., the *CR-cre* mice were injected with *AAV2/9-EF1α-DIO-eYFP* and received yellow light stimulation. We found that optogenetic inhibition of PIL CR neurons retarded seizure development (Figure 3D) and decreased the ADD (Figure 3E) during kindling-induced seizure acquisition. Inhibition of PIL CR neurons significantly increased the number of stimulations required to stay at stages 0-2; the overall number of stimulations
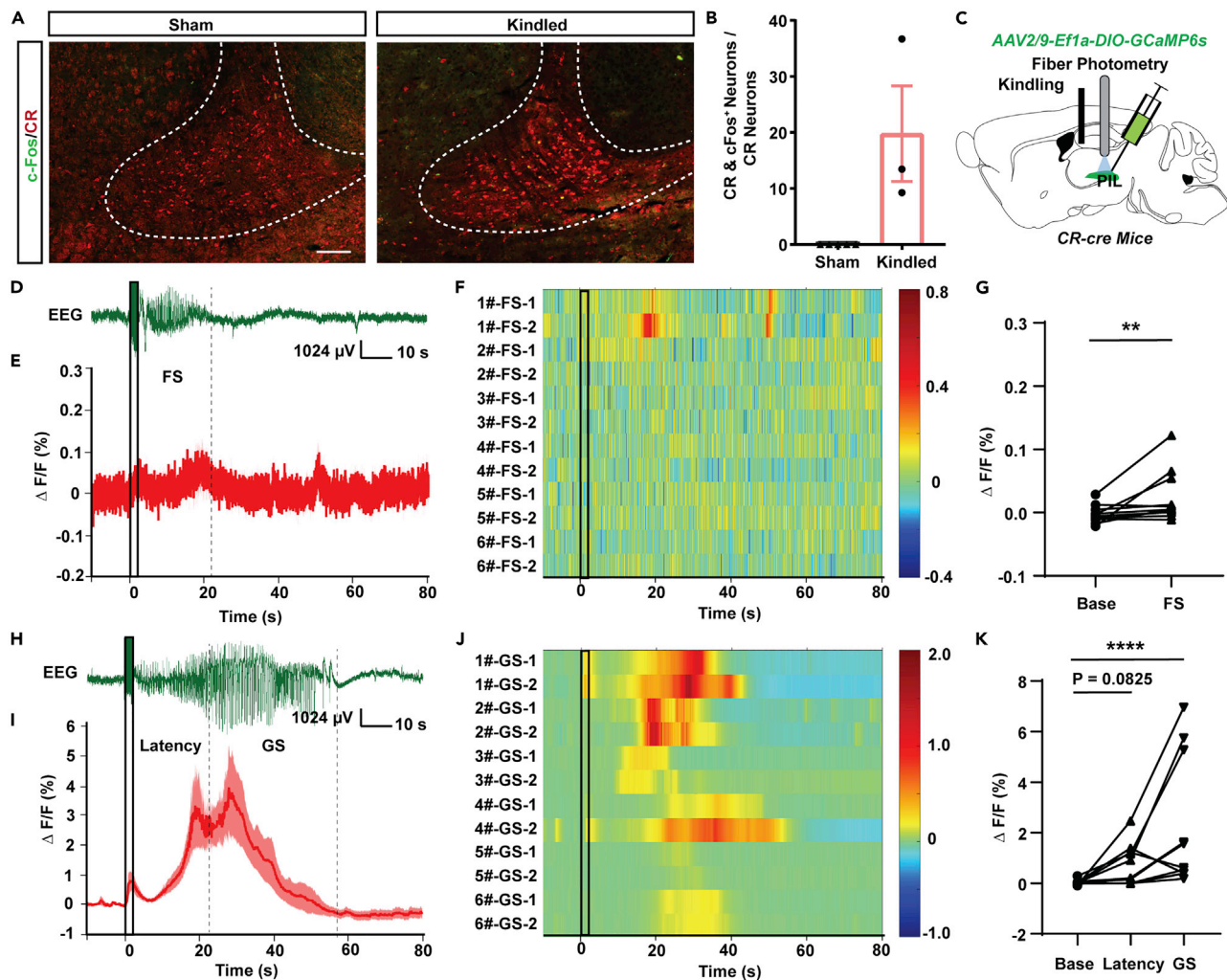
Figure 1. CR neurons in the PIL are activated during hippocampal seizures

(A) Representative images of immunofluorescence of colocalizations (yellow) of CR (red), c-Fos (green) in the PIL region of sham and kindled mice (Scale Bar: 100 μm).

(B) Percentages of CR^+ neurons expressing c-Fos in sham and kindled mice. Data are represented as mean ± SEM.

(C) Experimental schematic of the viral injection and photorecording of $CR\text{-}GCaMP6s^{PIL}$ mice. The $AAV2/9\text{-}Ef1a\text{-}DIO\text{-}GCaMP6s$ was injected into the PIL of $CR\text{-}cre$ mice.

(D) Representative EEG of a focal seizure (FS) in hippocampal kindling model. The black rectangles represent kindling stimulation.

(E) Fiber photometry of Ca^{2+} activities of PIL CR neurons during FS in PIL (n = 6 mice). Data are represented as mean ± SEM.

(F) Heatmap illustration of Ca^{2+} signals aligned to the initiation of stimulation. Each row represents the typical calcium signal of each trial during FS (6 mice, each mouse with two trials). Color scale indicates ΔF/F and warmer colors indicate higher fluorescence signal.

(G) Group data of trials showing quantification of the average ΔF/F during Base and FS of mice. "FS" is the average ΔF/F of the seizure duration (ADD period) and "Base" is average ΔF/F during 10 s before kindling stimulation. **p < 0.01, Wilcoxon test.

(H) Representative EEG of a generalized seizure (GS) in hippocampal kindling model.

(I) Fiber photometry of Ca^{2+} activities of PIL CR neurons during GS in PIL (n = 6 mice). Data are represented as mean ± SEM.

(J) Heatmap illustration of Ca^{2+} signals aligned to the initiation of stimulation. Each row represents the typical calcium signal of each trial during GSs (6 mice, each mouse with two trials). Color scale indicates ΔF/F and warmer colors indicate higher fluorescence signal.

(K) Group data of trials showing quantification of the average ΔF/F Ca^{2+} activity during Base, Latency to GS and GS states. ADD is separated into Latency to GS and GS according to the time mice rearing bilateral forelimbs. ****p < 0.0001, Friedman test.

required to achieve first stage 2 or 4 (GS) was also increased (Figures 3F and 3G). EEG and spectrum analysis demonstrated that mice given yellow light showed a drastic decrease in seizure intensity compared to mice given blue light (Figures 3H and 3I). Thus, the aforementioned results signify that PIL CR neurons are both required and necessary for the development of the hippocampal seizure.
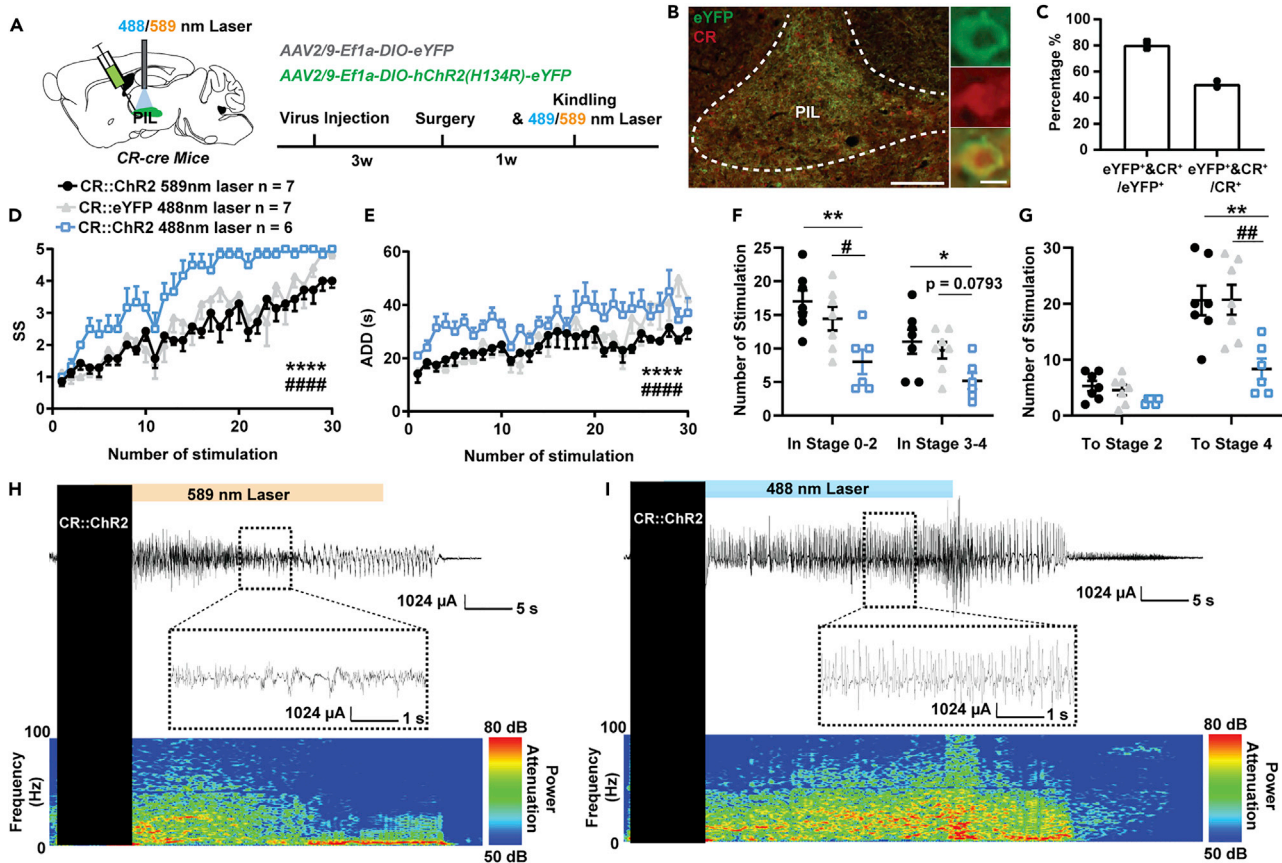
Figure 2. Optogenetic activation of CR neurons in the PIL promotes seizure progression

(A) Experimental schematic of viral injection and photostimulation in $CR\text{-}ChR2^{PIL}$ mice. $AAV2/9\text{-}EF1\alpha\text{-}DIO\text{-}hChR2(H134R)\text{-}eYFP$ was injected into the PIL of $CR\text{-}cre$ mice.

(B) Representative images of the PIL from a $CR\text{-}ChR2^{PIL}$ mouse, showing the overlap of eYFP and CR neurons (red). Scale Bar: 200 μm. Right, scaled up immunoreactivity image of eYFP, CR, and colocalization of both stains (yellow). Scale bar: 20 μm.

(C) Quantification of the percentage of eYFP neurons that co-express CR (n = 2). Data are represented as mean.

(D–G) Effects of optogenetic activation of PIL CR neurons on developmental seizure stage (SS, D), after-discharge duration (ADD, E), number of stimulations in different stages (F), and number of stimulations to different stages (G). The number of mice in each group is indicated in figure. *p < 0.05, **p < 0.01, ****p < 0.0001, compared with CR::ChR2 589 nm laser group; #p < 0.05, ##p < 0.01, ####p < 0.0001, compared with CR::eYFP 488 nm laser group; For D, E, two-way ANOVA with Dunnett's multiple comparisons test; For F and G, one-way ANOVA with Dunnett's multiple comparisons test. Data are represented as mean ± SEM.

(H and I) Representative EEGs and corresponding power spectra of mice.

Mapping the output projections of PIL CR neurons

Next, we investigated the downstream neural circuits of PIL CR neurons that play such a role in epilepsy. Firstly, we determined whether PIL CR neurons released excitatory or inhibitory neurotransmitters. Through immunostaining with CaMKIIa (a marker of excitatory glutamatergic neuron) and GAD65/67 (a marker of inhibitory GABAergic neuron), we found that there are about 75.60 ± 4.03% of CR neurons colocalized with CaMKIIa (Figures S2A–S2B), whereas almost no CR neuron colocalized with GAD65/67 (Figures S2C–S2D). This suggests that PIL CR neurons are glutamatergic neurons but not GABAergic neurons. Then, we map the projections of the PIL CR neurons by expressing $AAV2/9\text{-}CAG\text{-}FLEX\text{-}ArchT\text{-}GFP$ in the PIL of $CR\text{-}cre$ mice. We found that PIL CR neurons project to various downstream regions including the LA, ZI, auditory cortex, and central amygdaloid nucleus (Figures 4A and 4B). In addition, we monitored the c-Fos expression in these regions and verified that these regions have dense c-fos expressions after GS (Figure 4C). As the LA and ZI were found to have dense projections, we chose these two downstream circuits for further exploration.

Inhibition of PIL-LA CR circuit ameliorated hippocampal seizures

Similarly, we used optogenetics to selectively inhibit the PIL-LA CR circuit in the kindling model. $AAV2/9\text{-}CAG\text{-}FLEX\text{-}ArchT\text{-}GFP$ virus was injected into the PIL of $CR\text{-}cre$ mice and expressed for 5 weeks.
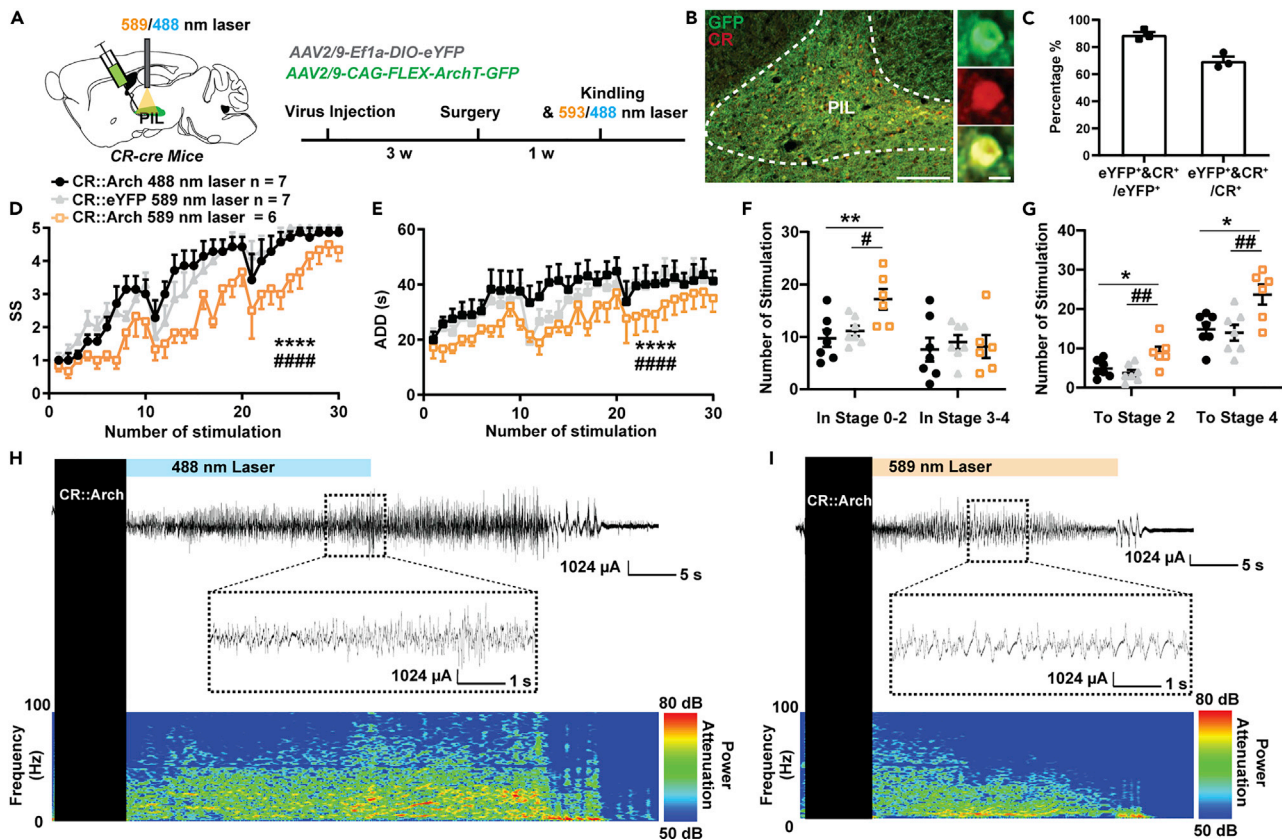
Figure 3. Optogenetic inhibition of CR neurons in the PIL retards seizure progression

(A) Experimental schematic of viral injection and photostimulation *CR-Arch^PIL* mice. *AAV2/9-CAG-FLEX-ArchT-GFP* was injected in the PIL of *CR-cre* mice.

(B) Representative images of the PIL from a *CR-Arch^PIL* mouse, showing the overlap of GFP and CR neurons (red). Scale Bar: 200 μm. Right, scaled up immunoreactivity image of GFP, CR, and colocalization of both stains (yellow). Scale bar: 20 μm.

(C) Quantification of the percentage of GFP neurons that co-express CR (n = 3). Data are represented as mean ± SEM.

(D–G) Effects of optogenetic inhibition of PIL CR neurons on developmental seizure stage (SS, D), after-discharge duration (ADD, E), number of stimulations in different seizure stage (F), number of stimulations to different seizure stage (G). The number of mice in each group is indicated in figure. *p < 0.05, **p < 0.01, ****p < 0.0001, compared with CR::Arch 488 nm laser group; #p < 0.05, ##p < 0.01, ####p < 0.0001, compared with CR::eYFP 589 nm laser group; For D, E, two-way ANOVA with Dunnett's multiple comparisons test; For F and G, one-way ANOVA with Dunnett's multiple comparisons test. Data are represented as mean ± SEM.

(H and I) Representative EEGs and corresponding power spectra of mice.

Electrodes and optic fiber were stereotaxically implanted into the CA3 region for and the LA, respectively (Figures 5A and 5B). We found that inhibiting PIL-LA CR circuit retarded seizure progression (Figure 5C) and shortened the ADD (Figure 5D) during kindling-induced seizure acquisition, mimicking the effects of optogenetic inhibition of PIL CR neurons. However, inhibition of PIL-LA CR circuit significantly increased the number of stimulations required to stay in both seizure stages 0-2 and 3-4; the overall number of stimulations required to achieve first stage 2 or 4 (GS) was also increased (Figures 5E and 5F), suggesting a stronger seizure-inhibition effect. This also indicated that propagation and maintenance of epileptic seizure might be mediated by distinct network mechanisms. EEG and spectrum analysis demonstrated that mice given yellow light showed a drastic decrease in seizure intensity compared to mice given blue light (Figures 5G and 5H). In addition, we tested whether inhibition of PIL-LA CR circuit would have an effect on GS in fully kindled state. After mice were fully kindled, optogenetic inhibition of PIL-LA CR circuit had no effect on seizure stage and ADD during GS expression (Figures S3A and S3B) but significantly shortened GSD (Figure S3C) and increased the latency to GS (Figure S3D). To sum up, these results demonstrate that optogenetic inhibition of the PIL-LA CR circuit shows stronger seizure-inhibition effect than direct inhibition of PIL CR neuron, and PIL-LA CR circuit plays a critical role in both kindling and kindled seizures.
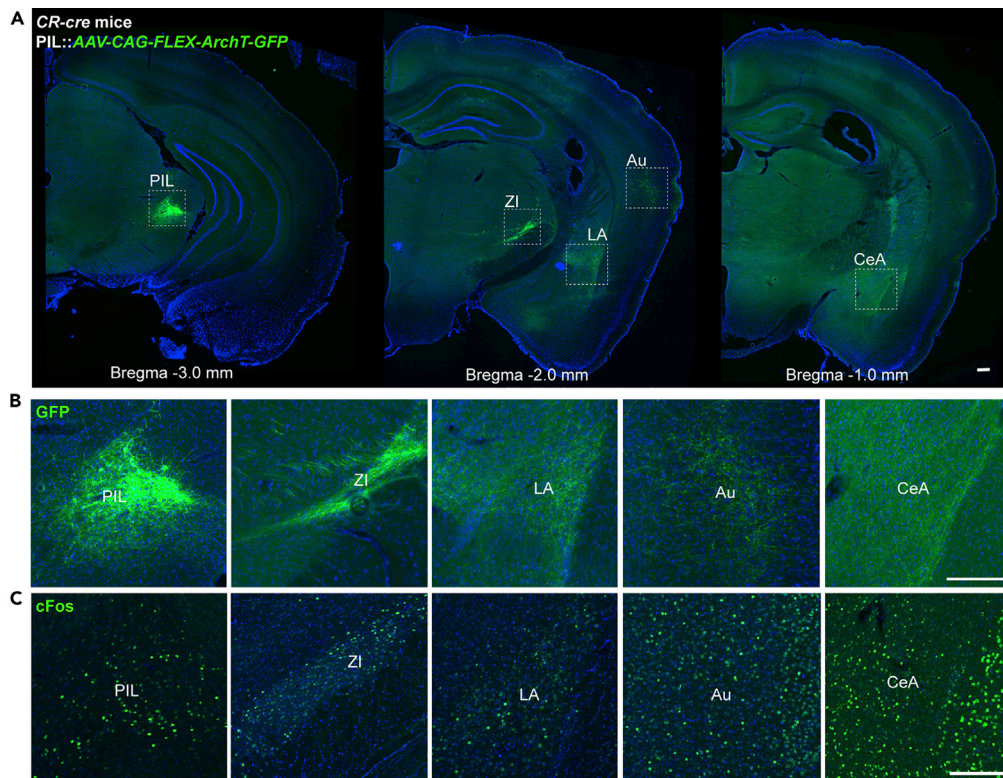
Figure 4. Mapping the main output regions of CR neurons in the PIL

(A) A series of representative images showing CR projections from a *CR-cre* mouse injected with *AAV2/9-CAG-FLEX-ArchT-GFP* into the PIL, illustrating the principal projections of the PIL CR neurons (left image). Scale bar: 1.0 mm.

B and C) Enlarged view of Arch-GFP soma within PIL and GFP$^+$ axon fibers in ZI, LA, Au, and CeA (B) and corresponding c-Fos expression after kindling-induced GS (C). Scale Bar: 200 μm. PIL, posterior intralaminar thalamic nucleus; Au, auditory cortex; LA, lateral amygdala; CeA, central amygdaloid nucleus; ZI, zona incerta.

Inhibition of PIL-ZI CR circuit proliferated hippocampal seizures

Next, we used optogenetics to selectively inhibit the PIL-ZI CR circuit in the kindling model. *AAV2/9-CAG-FLEX-ArchT-GFP* virus was injected into the PIL of *CR-cre* mice and expressed for 5 weeks. Electrodes and optic fiber were stereotaxically implanted into the CA3 region and the ZI, respectively (Figures 6A and 6B). Amazingly, we found that inhibiting the PIL-ZI CR circuit showed a totally different role in seizure acquisition, with accelerating seizure progression (Figure 6C) and increasing the ADD (Figure 6D). Inhibition of PIL-ZI CR circuit decreased the number of stimulations required to stay in stages 0-2 and 3-4; the overall number of stimulations required to achieve GS (stage 4) was also decreased (Figures 6E and 6F). EEG and spectrum analysis demonstrated that mice given yellow light showed a drastic decrease in seizure intensity compared to mice given blue light (Figures 6G and 6H). In addition, we tested whether inhibition of PIL-ZI CR circuit would have an effect on GS in fully kindled state. After mice were fully kindled, optogenetic inhibition of PIL-ZI CR circuit had no effect on seizure stage, ADD, and latency to GS but increased the GSD (Figures S4A–S4D). These results demonstrate that optogenetic inhibition of the PIL-ZI CR circuit, which plays an opposite role in epilepsy compared with that of PIL-LA CR circuit, aggravated hippocampal seizure. Finally, we aimed to test whether LA-projecting and ZI-projecting CR neurons are separated subpopulations in the PIL. *AAV2/2Retro-hEF1a-DIO-eYFP* and *AAV2/2Retro-hEF1a-DIO-mCherry* are injected into the LA and ZI region, respectively, and allowed to retrograde back to PIL region. In representative images, the eFYP$^+$ neurons indicate LA-projecting CR neurons, the mCherry$^+$ neurons indicate ZI-projecting CR neurons, and yellow neurons (white arrows) indicate collateral projecting CR neurons (Figure 7A). Interestingly, statistical data showed a large proportion of overlap of LA-projecting and ZI-projecting CR neurons in the PIL, which accounts for ~42.67% ZI-projecting CR neurons and ~70.4% LA-projecting CR neurons (Figures 7B and 7C). This result indicates that LA-projecting and ZI-projecting CR neurons show partial overlap in the PIL.
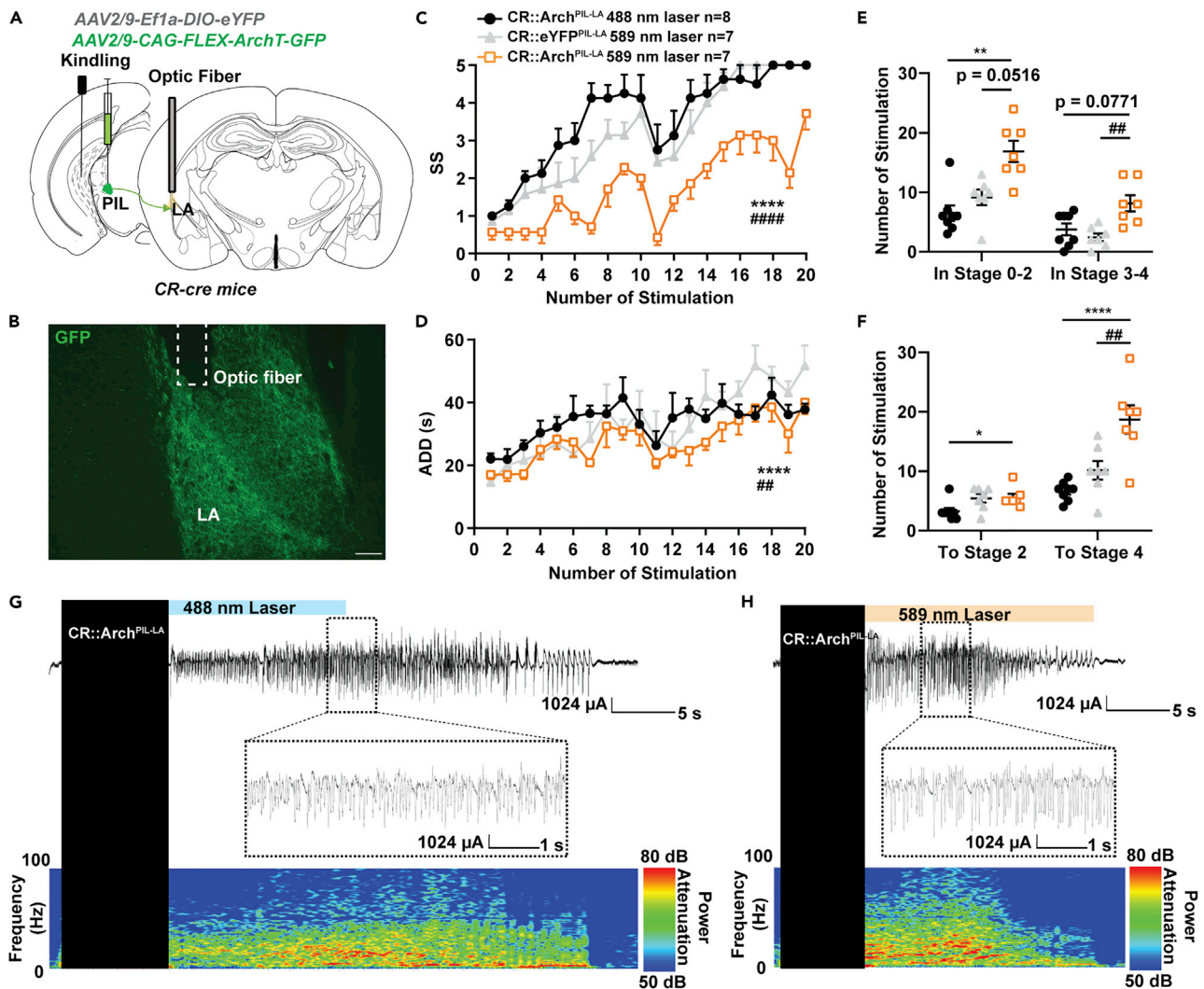
Figure 5. Inhibition of PIL-LA CR circuit impedes hippocampal seizure

(A) Experimental schematic diagram of optogenetic inhibition of the PIL-LA CR projections in *CR-Arch^{PIL}* mice.

(B) Representative image showing the Arch-GFP axon fibers within the LA projected from the PIL and the optic fiber (dotted line). Scale bar: 200 μm.

(C–F) Effects of optogenetic inhibition of PIL-LA CR projections on seizure stage (SS, C), after-discharge duration (ADD, D), the number of stimulations in seizure stages (E), and the number of stimulations needed to reach each stage (F). The number of mice in each group is indicated in figure. *p < 0.05, **p < 0.01, ****p < 0.0001, compared with CR::Arch^{PIL-LA} 488nm laser group; ##p < 0.01, ####p < 0.0001, compared with CR::eYFP^{PIL-LA} 589nm laser group; For C, D, two-way ANOVA with Dunnett's multiple comparisons test; For E, Kruskal-Wallis test with Dunn's multiple comparisons test; For F, one-way ANOVA with Dunnett's multiple comparisons test. Data are represented as mean ± SEM.

(G and H) Representative EEGs and corresponding power spectra of mice.

DISCUSSION

Previous studies demonstrated that CR neurons have altered morphologies (Magloczky and Freund, 2005; Toth et al., 2010) and numbers (Blumcke et al., 1996, 1999; Buckmaster et al., 2017; Ma et al., 2006; Thom et al., 2002; Zhang et al., 2009) in various brain regions after epilepsy, although the causality is unknown. In this study, we found that the number of CR neurons was not significantly changed after hippocampal kindling seizure, but the activity of PIL CR neurons was significantly increased after GS. Optogenetically activating the PIL CR neurons accelerated epilepsy progression, whereas inhibiting PIL CR neurons delayed the progression of epilepsy. In addition, PIL CR neurons were found to be projecting glutamatergic neurons. Selectively inhibiting the PIL-LA CR circuit produced a stronger antiepileptic effect than directly inhibiting the CR neurons in the PIL region, whereas selectively inhibiting the PIL-ZI CR circuit accelerated
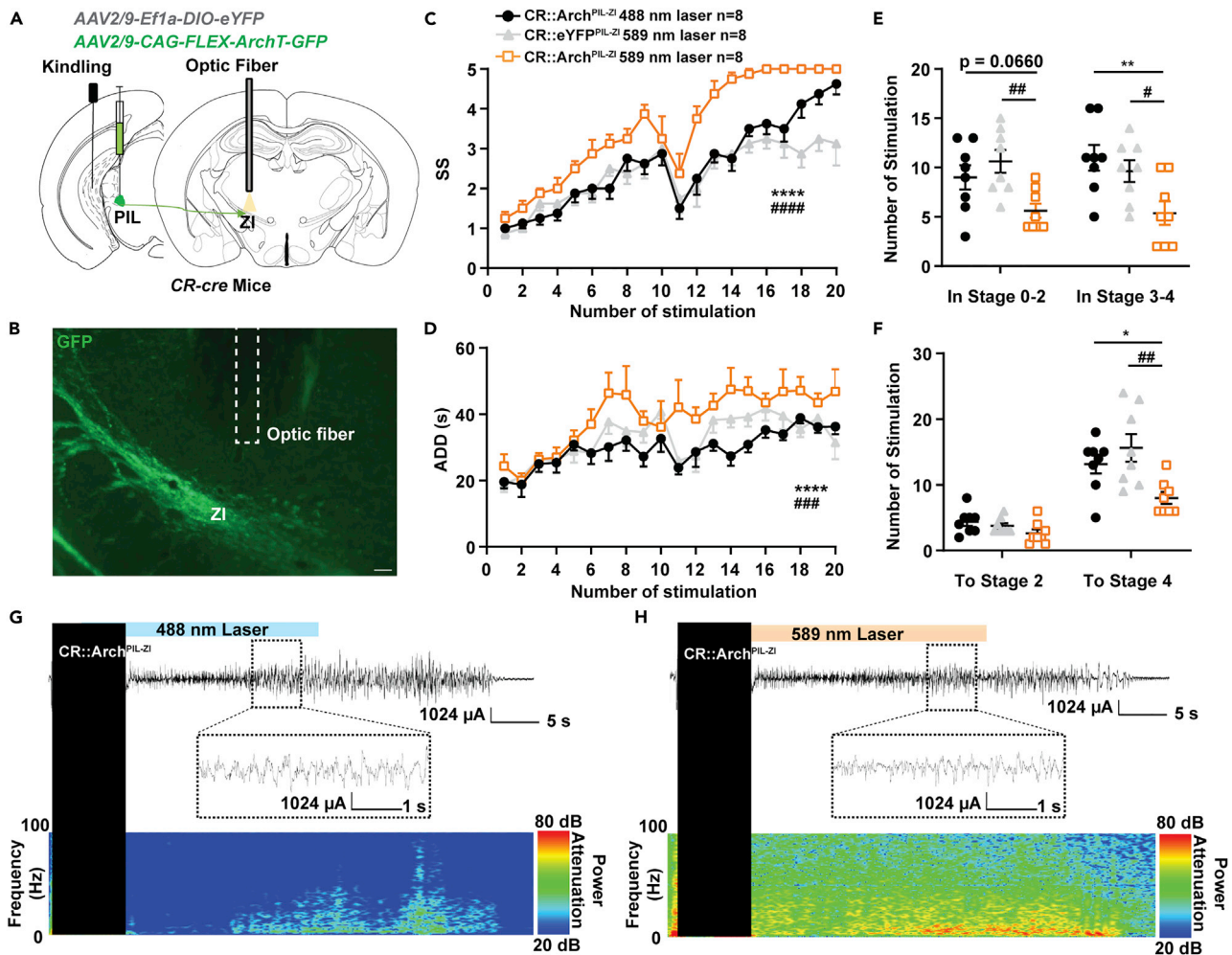
Figure 6. Inhibition of PIL-ZI CR circuit proliferates hippocampal seizure

(A) Experimental schematic diagram optogenetic inhibition of the PIL-ZI CR projections in *CR-Arch[PIL]* mice.

(B) Representative image showing the Arch-GFP axon fibers within the ZI projected from the PIL and the optic fiber (dotted line). Scale bar: 200 μm.

(C–F) Effects of optogenetic inhibition of PIL-ZI CR projections on seizure stage (SS, C), after-discharge duration (ADD, D), the number of stimulations in seizure stages (E), and the number of stimulations needed to reach each stage (F). The number of mice in each group is indicated in figure. *p < 0.05, **p < 0.01, ****p < 0.0001, compared with CR::Arch[PIL−ZI] 488nm laser group; #p < 0.05, ##p < 0.01, ###p < 0.001, ####p < 0.0001, compared with CR::eYFP[PIL−ZI] 589nm laser group; For C, D, two-way ANOVA with Dunnett's multiple comparisons test; For E, Kruskal-Wallis test with Dunn's multiple comparisons test; For F, one-way ANOVA with Dunnett's multiple comparisons test. Data are represented as mean ± SEM.

(G and H) Representative EEGs and corresponding power spectra (H) of mice.

epilepsy progression. In conclusion, PIL CR neurons play an important but diverse role in hippocampal seizure via distinct downstream neural circuits.

Mapping of CR neuron and its changes in hippocampal kindling model

In prior research, CR neurons were found to have various morphological and physiological changes in different brain regions of epilepsy models. Vulnerability of CR neurons in epileptic patients was theorized to be a contributor to epileptogenesis (Toth et al., 2010). However, contradictory research has shown an increased immunoreactivity of Cajal-Retzius CR cells in the hippocampus of TLE patients with sclerosis (Blumcke et al., 1996; Thom et al., 2002). In this study, mapping of the CR neurons was used to observe the changes of CR neurons in various brain regions after hippocampal kindling seizure. Unlike the prior publication that found altered numbers of CR neurons in various brain regions (Botterill et al., 2017), we found no changes to the amount of CR present between the sham group and the hippocampal-kindled group. This may be explained by the fact that the kindling model is generally considered as a gentler model
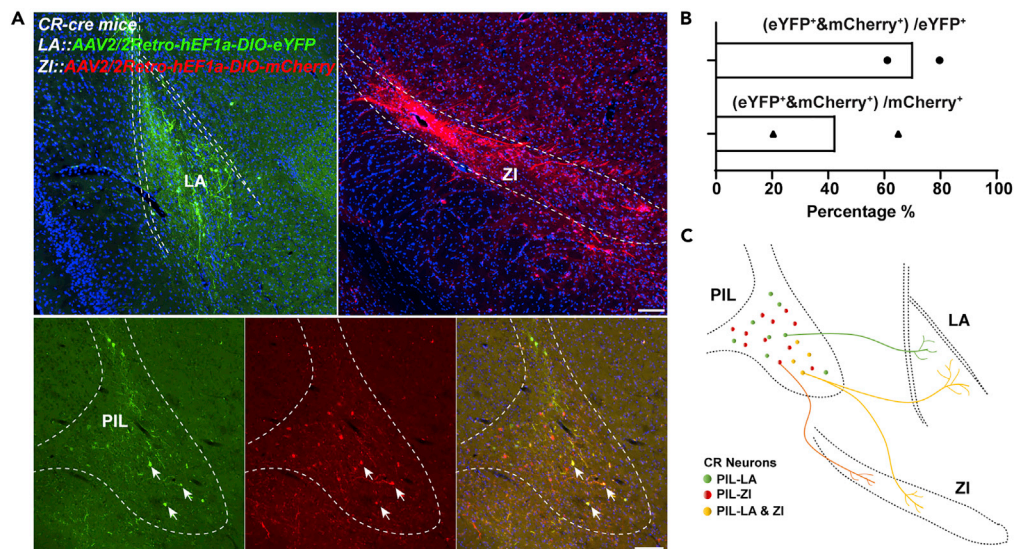
Figure 7. LA- and ZI-projecting CR neurons show partial overlap in the PIL

(A) Representative images showing the overlap of LA-projecting and ZI-projecting CR neurons in the PIL. *AAV2/2Retro-hEF1a-DIO-eYFP* and *AAV2/2Retro-hEF1a-DIO-mCherry* were injected into the LA and ZI regions, respectively, and allowed to retrograde back to the PIL region. The eFYP^{+} neurons indicate LA-projecting CR neurons, the mCherry^{+} neurons indicate ZI-projecting CR neurons, and the yellow neurons (white arrows) indicate collateral-projecting CR neurons. Scale Bar: 200 μm.

(B) Statistical data of overlap percentage of LA-projecting and ZI-projecting CR neurons in the PIL from two mice. Data are represented as mean.

(C) Graphical representation of LA-projecting and ZI-projecting CR neurons showing partial overlap in the PIL.

with lesser degrees of tissue damage compared with drug-induced epilepsy models such as kainate or pilocarpine. This also suggests that the loss of CR neurons may not be a determinative factor for seizure development. An explanation to CR's decrease in kindling epilepsy in Botterill's paper was because of the extreme parameters used in the kindling model, resulting in increased neuronal death because of excitotoxicity (Botterill et al., 2017). Mapping of c-Fos expression—a marker for neuronal activity (Bullitt, 1990; Ivashkina et al., 2021)—after GS revealed that a significant portion of CR neurons are activated in many regions of the brain, including the PIL. In addition, Ca^{2+} fiber photometry (Broussard and Petreanu, 2021) suggested that PIL CR neurons are significantly activated during GS but not FS in hippocampal kindling model. These results signify that PIL CR neurons play an important role in hippocampal seizure progression and propagation.

Functionality of PIL CR neurons in epilepsy

CR neurons and its functionality during epilepsy are currently unknown. In prior research, it was hypothesized that CR neurons can activate inhibitory neurons through synchronous firing, thereby suppressing pyramidal neurons (Toth et al., 2010). However, we found that activating PIL CR neurons significantly hastened seizure progression, whereas inhibiting PIL CR neurons significantly retarded seizure development mainly during the early stage, which further supports the notion that PIL CR neurons play an important role in seizure progression. Owing to the projecting nature of CR neurons in the PIL region, it may contribute to the propagation of seizures by activating the downstream circuits. In prior reports, CR neurons have also been described to functionally disinhibit pyramidal neurons through inhibiting other inhibitory neurons (McDonald and Mascagni, 2001; Sorvari et al., 1998). In addition, we found that PIL CR neurons are projecting glutamatergic neurons but not local GABAergic neurons, and it may have an effect on the seizure progression through different downstream circuits involved in excitatory neurotransmission.

Opposing effects are present in PIL CR circuits

The LA and ZI are regions of the brain are associated in different types of seizures (Hamani et al., 2002; Mihaly et al., 2020; Wang et al., 2014). Here, we verified that both LA and ZI exhibited dense c-Fos expression,

implying they are active during seizure. Optogenetic modulation of these two circuits showed surprisingly paradoxical effects on hippocampal seizures. Selective inhibition of the PIL-LA CR circuit produced a stronger antiepileptic effect than direct inhibition the PIL CR neurons, especially in stage 3-4. To the contrary, selective inhibition of the PIL-ZI CR circuit elicited the opposite effect, hastening epilepsy progression. In addition, retrograde viral tracing showed that LA-projecting and ZI-projecting CR neurons partially overlap in the PIL. Thus, there may be one possible reason for this result: one same group of CR neurons in PIL play the opposite role in epilepsy by collateral projections regulating different downstream circuits. It can be proposed that a distinct postsynaptic mechanism at the target regions and/or some level of homeostatic balance in the system is provided by the collateral PIL pathway, thus endogenously regulating the excitation inhibition balance in the brain. In addition, further investigations are needed to find out whether other downstream brain regions of PIL CR neurons are involved in seizure control. As an example, the PIL also directly projects to the neighboring striatal regions (Figure 4), and PIL may also disynaptically influence striatal regions that received strong projects from the LA; thus, it is worth to study whether the PIL is able to control epileptic event through its direct or indirect connections to the basal ganglia system.

In conclusion, we demonstrated that PIL CR neurons play a critical but heterogeneous role in hippocampal seizures, and there exist two different PIL CR circuits that have opposing functions in epilepsy. Therefore, a circuit-level treatment should be considered as the precise medicine for epilepsy.

Limitations of the study

As already noted, we confirmed that PIL CR neurons play a critical but heterogeneous role in hippocampal seizures of kindling model; however, whether PIL CR neurons would play a similar role in other chronic epilepsy models, such as pilocarpine-induced chronic spontaneous seizures, is still unknown. Unexpectedly, there was a different epileptogenic susceptibility of control groups in the optogenetic experiment (Figure S6), which might be because of factors such as different color with light stimulation or the minor injuries caused by the implantation of optic fiber at the different locations. This could be a potential confound of the study that needs to be taken into consideration when interpreting whether different areas modulate seizures. In addition, we are still far from clear on how CR neurons in other areas of the brain, such as CR neurons in cortex and hippocampus, function in epilepsy, and this needs to be further investigated.

STAR★METHODS

Detailed methods are provided in the online version of this paper and include the following:

- KEY RESOURCES TABLE
- RESOURCE AVAILABILITY
  - Lead contact
  - Materials availability
  - Data and code availability
- EXPERIMENTAL MODEL AND SUBJECT DETAILS
  - Animals
  - Virus
- METHOD DETAILS
  - Stereotaxic surgery
  - *In vivo* fiber photometry
  - Kindling model
  - Optogenetic modulation
  - Immunohistochemistry
- QUANTIFICATION AND STATISTICAL ANALYSIS

SUPPLEMENTAL INFORMATION

Supplemental information can be found online at https://doi.org/10.1016/j.isci.2022.104218.

ACKNOWLEDGMENTS

AUTHOR CONTRIBUTIONS

DECLARATION OF INTERESTS

REFERENCES

Barsy, B., Kocsis, K., Magyar, A., Babiczky, A., Szabo, M., Veres, J.M., Hillier, D., Ulbert, I., Yizhar, O., and Matyas, F. (2020). Associative and plastic thalamic signaling to the lateral amygdala controls fear behavior. Nat. Neurosci. 23, 625–637. https://doi.org/10.1038/s41593-020-0620-z.

Benini, R., and Avoli, M. (2006). Altered inhibition in lateral amygdala networks in a rat model of temporal lobe epilepsy. J. Neurophysiol. 95, 2143–2154. https://doi.org/10.1152/jn.01217.2005.

Bialer, M., and White, H.S. (2010). Key factors in the discovery and development of new antiepileptic drugs. Nat. Rev. Drug Discov. 9, 68–82. https://doi.org/10.1038/nrd2997.

Blumcke, I., Beck, H., Nitsch, R., Eickhoff, C., Scheffler, B., Celio, M.R., Schramm, J., Elger, C.E., Wolf, H.K., and Wiestler, O.D. (1996). Preservation of calretinin-immunoreactive neurons in the hippocampus of epilepsy patients with Ammon's horn sclerosis. J. Neuropathol. Exp. Neurol. 55, 329–341. https://doi.org/10.1097/00005072-199603000-00008.

Blumcke, I., Beck, H., Suter, B., Hoffmann, D., Fodisch, H.J., Wolf, H.K., Schramm, J., Elger, C.E., and Wiestler, O.D. (1999). An increase of hippocampal calretinin-immunoreactive neurons correlates with early febrile seizures in temporal lobe epilepsy. Acta Neuropathol. 97, 31–39. https://doi.org/10.1007/s004010050952.

Botterill, J.J., Nogovitsyn, N., Caruncho, H.J., and Kalynchuk, L.E. (2017). Selective plasticity of hippocampal GABAergic interneuron populations following kindling of different brain regions. J. Comp. Neurol. 525, 389–406. https://doi.org/10.1002/cne.24071.

Broussard, G.J., and Petreanu, L. (2021). Eavesdropping wires: recording activity in axons using genetically encoded calcium indicators. J. Neurosci. Methods 360, 109251. https://doi.org/10.1016/j.jneumeth.2021.109251.

Buckmaster, P.S., Abrams, E., and Wen, X. (2017). Seizure frequency correlates with loss of dentate gyrus GABAergic neurons in a mouse model of temporal lobe epilepsy. J. Comp. Neurol. 525, 2592–2610. https://doi.org/10.1002/cne.24226.

Bullitt, E. (1990). Expression of c-fos-like protein as a marker for neuronal activity following noxious stimulation in the rat. J. Comp. Neurol. 296, 517–530. https://doi.org/10.1002/cne.902960402.

Chen, B., Xu, C., Wang, Y., Lin, W., Wang, Y., Chen, L., Cheng, H., Xu, L., Hu, T., Zhao, J., et al. (2020). A disinhibitory nigra-parafascicular pathway amplifies seizure in temporal lobe epilepsy. Nat. Commun. 11, 923. https://doi.org/10.1038/s41467-020-14648-8.

Cheng, H., Qi, Y., Lai, N., Yang, L., Xu, C., Wang, S., Guo, Y., Chen, Z., and Wang, Y. (2021). Inhibition of hyperactivity of the dorsal raphe 5-HTergic neurons ameliorates hippocampal seizure. CNS Neurosci. Ther. 27, 963–972. https://doi.org/10.1111/cns.13648.

Cheng, H., Wang, Y., Chen, J., and Chen, Z. (2020). The piriform cortex in epilepsy: what we learn from the kindling model. Exp. Neurol. 324, 113137. https://doi.org/10.1016/j.expneurol.2019.113137.

Drexel, M., Preidt, A.P., Kirchmair, E., and Sperk, G. (2011). Parvalbumin interneurons and calretinin fibers arising from the thalamic nucleus reuniens degenerate in the subiculum after kainic acid-induced seizures. Neuroscience 189, 316–329. https://doi.org/10.1016/j.neuroscience.2011.05.021.

Fialho, G.L., Pagani, A.G., Wolf, P., Walz, R., and Lin, K. (2018). Echocardiographic risk markers of sudden death in patients with temporal lobe epilepsy. Epilepsy Res. 140, 192–197. https://doi.org/10.1016/j.eplepsyres.2018.01.016.

Fiest, K.M., Dykeman, J., Patten, S.B., Wiebe, S., Kaplan, G.G., Maxwell, C.J., Bulloch, A.G., and Jette, N. (2013). Depression in epilepsy: a systematic review and meta-analysis. Neurology 80, 590–599. https://doi.org/10.1212/WNL.0b013e31827b1ae0.

Fonseca, M., del Rio, J.A., Martinez, A., Gomez, S., and Soriano, E. (1995). Development of calretinin immunoreactivity in the neocortex of the rat. J. Comp. Neurol. 361, 177–192. https://doi.org/10.1002/cne.903610114.

Franzini, A., Messina, G., Marras, C., Villani, F., Cordella, R., and Broggi, G. (2008). Deep brain stimulation of two unconventional targets in refractory non-resectable epilepsy. Stereotact. Funct. Neurosurg. 86, 373–381. https://doi.org/10.1159/000175800.

Gonchar, Y., and Burkhalter, A. (2003). Distinct GABAergic targets of feedforward and feedback connections between lower and higher areas of rat visual cortex. J. Neurosci. 23, 10904–10912.

Hamani, C., Sakabe, S., Bortolotto, Z.A., Cavalheiro, E.A., and Mello, L.E. (2002). Inhibitory role of the zona incerta in the pilocarpine model of epilepsy. Epilepsy Res. 49, 73–80. https://doi.org/10.1016/s0920-1211(02)00017-7.

Ivashkina, O.I., Gruzdeva, A.M., Roshchina, M.A., Toropova, K.A., and Anokhin, K.V. (2021). Imaging of C-fos activity in neurons of the mouse parietal association cortex during acquisition and retrieval of associative fear memory. Int. J. Mol. Sci. 22, 8244. https://doi.org/10.3390/ijms22158244.

Kita, T., Shigematsu, N., and Kita, H. (2016). Intralaminar and tectal projections to the subthalamus in the rat. Eur. J. Neurosci. 44, 2899–2908. https://doi.org/10.1111/ejn.13413.

Lin, J.J., Mula, M., and Hermann, B.P. (2012). Uncovering the neurobehavioural comorbidities of epilepsy over the lifespan. Lancet 380, 1180–1192. https://doi.org/10.1016/S0140-6736(12)61455-X.

Linke, R. (1999). Organization of projections to temporal cortex originating in the thalamic posterior intralaminar nucleus of the rat. Exp. Brain Res. 127, 314–320. https://doi.org/10.1007/s002210050801.

Liu, G., Slater, N., and Perkins, A. (2017). Epilepsy: treatment options. Am. Fam. Physician 96, 87–96.

Loscher, W., Potschka, H., Sisodiya, S.M., and Vezzani, A. (2020). Drug resistance in epilepsy: clinical impact, potential mechanisms, and new innovative treatment options. Pharmacol. Rev. 72, 606–638. https://doi.org/10.1124/pr.120.019539.

Ma, D.L., Tang, Y.C., Chen, P.M., Chia, S.C., Jiang, F.L., Burgunder, J.M., Lee, W.L., and Tang, F.R. (2006). Reorganization of CA3 area of the mouse hippocampus after pilocarpine induced temporal lobe epilepsy with special reference to the CA3-septum pathway. J. Neurosci. Res. 83, 318–331. https://doi.org/10.1002/jnr.20731.

Magloczky, Z., and Freund, T.F. (2005). Impaired and repaired inhibitory circuits in the epileptic human hippocampus. Trends Neurosci. 28,

334–340. https://doi.org/10.1016/j.tins.2005.04.002.

McDonald, A.J., and Mascagni, F. (2001). Colocalization of calcium-binding proteins and GABA in neurons of the rat basolateral amygdala. Neuroscience *105*, 681–693. https://doi.org/10.1016/s0306-4522(01)00214-7.

Mihaly, I., Orban-Kis, K., Gall, Z., Berki, A.J., Bod, R.B., and Szilagyi, T. (2020). Amygdala low-frequency stimulation reduces pathological phase-amplitude coupling in the pilocarpine model of epilepsy. Brain Sci. *10*, 856. https://doi.org/10.3390/brainsci10110856.

Percie du Sert, N., Hurst, V., Ahluwalia, A., Alam, S., Avey, M.T., Baker, M., Browne, W.J., Clark, A., Cuthill, I.C., Dirnagl, U., et al. (2020). The ARRIVE guidelines 2.0: updated guidelines for reporting animal research. BMJ Open Sci. *4*, e100115. https://doi.org/10.1136/bmjos-2020-100115.

Pfeffer, C.K., Xue, M., He, M., Huang, Z.J., and Scanziani, M. (2013). Inhibition of inhibition in visual cortex: the logic of connections between molecularly distinct interneurons. Nat. Neurosci. *16*, 1068–1076. https://doi.org/10.1038/nn.3446.

Qi, Y., Cheng, H., Wang, Y., and Chen, Z. (2021). Revealing the precise role of calretinin neurons in epilepsy: we are on the way. Neurosci. Bull. *38*, 209–222. https://doi.org/10.1007/s12264-021-00753-1.

Racine, R.J. (1972). Modification of seizure activity by electrical stimulation. II. Motor seizure. Electroencephalogr. Clin. Neurophysiol. *32*, 281–294. https://doi.org/10.1016/0013-4694(72)90177-0.

Saffari, R., Grotefeld, K., Kravchenko, M., Zhang, M., and Zhang, W. (2019). Calretinin(+)-neurons-mediated GABAergic inhibition in mouse prefrontal cortex. Prog. Neuropsychopharmacol. Biol. Psychiatry. *94*, 109658. https://doi.org/10.1016/j.pnpbp.2019.109658.

Schiffmann, S.N., Cheron, G., Lohof, A., d'Alcantara, P., Meyer, M., Parmentier, M., and Schurmans, S. (1999). Impaired motor coordination and purkinje cell excitability in mice lacking calretinin. Proc. Natl. Acad. Sci. U S A. *96*, 5257–5262. https://doi.org/10.1073/pnas.96.9.5257.

Sorvari, H., Miettinen, R., Soininen, H., Paljarvi, L., Karkola, K., and Pitkanen, A. (1998). Calretinin-immunoreactive terminals make synapses on calbindin D28k-immunoreactive neurons in the lateral nucleus of the human amygdala. Brain Res. *783*, 355–358. https://doi.org/10.1016/s0006-8993(97)01295-x.

Stephen, L.J., Wishart, A., and Brodie, M.J. (2017). Psychiatric side effects and antiepileptic drugs: observations from prospective audits. Epilepsy Behav. *71*, 73–78. https://doi.org/10.1016/j.yebeh.2017.04.003.

Thom, M., Sisodiya, S.M., Beckett, A., Martinian, L., Lin, W.R., Harkness, W., Mitchell, T.N., Craig, J., Duncan, J., and Scaravilli, F. (2002). Cytoarchitectural abnormalities in hippocampal sclerosis. J. Neuropathol. Exp. Neurol. *61*, 510–519. https://doi.org/10.1093/jnen/61.6.510.

Toth, K., Eross, L., Vajda, J., Halasz, P., Freund, T.F., and Magloczky, Z. (2010). Loss and reorganization of calretinin-containing interneurons in the epileptic human hippocampus. Brain *133*, 2763–2777. https://doi.org/10.1093/brain/awq149.

Toth, K., and Magloczky, Z. (2014). The vulnerability of calretinin-containing hippocampal interneurons to temporal lobe epilepsy. Front. Neuroanat. *8*, 100. https://doi.org/10.3389/fnana.2014.00100.

Wang, Y., and Chen, Z. (2019). An update for epilepsy research and antiepileptic drug development: toward precise circuit therapy. Pharmacol. Ther. *201*, 77–93. https://doi.org/10.1016/j.pharmthera.2019.05.010.

Wang, Y., Liang, J., Xu, C., Wang, Y., Kuang, Y., Xu, Z., Guo, Y., Wang, S., Gao, F., and Chen, Z. (2016). Low-frequency stimulation in anterior nucleus of thalamus alleviates kainate-induced chronic epilepsy and modulates the hippocampal EEG rhythm. Exp. Neurol. *276*, 22–30. https://doi.org/10.1016/j.expneurol.2015.11.014.

Wang, Y., Wang, Y., Xu, C., Wang, S., Tan, N., Chen, C., Chen, L., Wu, X., Fei, F., Cheng, H., et al. (2020). Direct septum-hippocampus cholinergic circuit attenuates seizure through driving somatostatin inhibition. Biol. Psychiatry *87*, 843–856. https://doi.org/10.1016/j.biopsych.2019.11.014.

Wang, Y., Xu, C., Xu, Z., Ji, C., Liang, J., Wang, Y., Chen, B., Wu, X., Gao, F., Wang, S., et al. (2017). Depolarized GABAergic signaling in subicular microcircuits mediates generalized seizure in temporal lobe epilepsy. Neuron *95*, 1221. https://doi.org/10.1016/j.neuron.2017.08.013.

Wang, Y., Xu, Z., Cheng, H., Guo, Y., Xu, C., Wang, S., Zhang, J., Ding, M., and Chen, Z. (2014). Low-frequency stimulation inhibits epileptogenesis by modulating the early network of the limbic system as evaluated in amygdala kindling model. Brain Struct. Funct. *219*, 1685–1696. https://doi.org/10.1007/s00429-013-0594-7.

Xu, C.L., Nao, J.Z., Shen, Y.J., Gong, Y.W., Tan, B., Zhang, S., Shen, K.X., Sun, C.R., Wang, Y., and Chen, Z. (2021). Long-term music adjuvant therapy enhances the efficacy of sub-dose antiepileptic drugs in temporal lobe epilepsy. CNS Neurosci. Ther. https://doi.org/10.1111/cns.13623.

Xu, Z., Wang, Y., Chen, B., Xu, C., Wu, X., Wang, Y., Zhang, S., Hu, W., Wang, S., Guo, Y., et al. (2016). Entorhinal principal neurons mediate brain-stimulation treatments for epilepsy. EBioMedicine *14*, 148–160. https://doi.org/10.1016/j.ebiom.2016.11.027.

Zhang, S., Khanna, S., and Tang, F.R. (2009). Patterns of hippocampal neuronal loss and axon reorganization of the dentate gyrus in the mouse pilocarpine model of temporal lobe epilepsy. J. Neurosci. Res. *87*, 1135–1149. https://doi.org/10.1002/jnr.21941.

STAR★METHODS

KEY RESOURCES TABLE

REAGENT or RESOURCE	SOURCE	IDENTIFIER
Antibodies		
Anti-CaMKII	Abcam	Cat#ab22609; RRID: AB_447192
Anti-GAD65/67	Millipore	Cat#AB1511; RRID: AB_90715
Anti-Calretinin	SWANT	Cat#7697; RRID: AB_2619710
Anti-cFos	Santa Cruz	Cat# sc-166940; RRID: AB_10609634
Anti-GFP	Abcam	Cat# ab1218; RRID: AB_298911
Donkey anti-mouse Alexa 488 secondary antibody	Jackson Immuno Research Laboratories	Cat#715-545-150; RRID: AB_2340846
Donkey anti-rabbit Alexa 594 secondary antibody	Jackson Immuno Research Laboratories	Cat#711-585-152; RRID: AB_2340621
Bacterial and virus strains		
AAV2/9-EF1a-DIO-GCaMP6s	OBiO Technology Co., Ltd	N/A
AAV2/9-Ef1α-DIO-hChR2(H134R)-eYFP	Taitool Bioscience Co., Ltd	N/A
AAV2/9-Ef1α-DIO-eYFP	OBiO Technology Co., Ltd	N/A
AAV2/9-CAG-FLEX-ArchT-GFP	OBiO Technology Co., Ltd	N/A
AAV2/2Retro-hEF1α-DIO-EYFP	Taitool Bioscience Co., Ltd	N/A
AAV2/2Retro-hEF1α-DIO-mCherry	Taitool Bioscience Co., Ltd	N/A
Experimental models: Organisms/strains		
Mouse: B6(Cg)-Calb2tm1(cre)Zjh/J	The Jackson Laboratory	RRID: IMSR_JAX:010,774
Software and algorithms		
PRISM	GraphPad Software	RRID: SCR_002798
ImageJ	NIH	RRID: SCR_003070
Olympus VS120	Olympus	RRID: SCR_018411

RESOURCE AVAILABILITY

Lead contact

Further information and requests for resources and reagents should be directed to and will be fulfilled by the Lead Contact, Yi Wang (wang-yi@zju.edu.cn).

Materials availability

This study did not generate any new unique reagents.

Data and code availability

- All data reported in this paper will be shared by the lead contact upon request.

- This paper does not report original code.

- Any additional information required to reanalyze the data reported in this paper is available from the lead contact upon request.

EXPERIMENTAL MODEL AND SUBJECT DETAILS

Animals

B6(Cg)-Calb2[tm1(cre)Zjh] mice (*CR-cre* mice, stock No.010774) were genotyped according to the protocols provided by Jackson Laboratory and were bred with C57BL/6J mice. Male *CR-cre* mice and C57BL/6J mice (at least 2 months old and weighing of approximately 20-30g) were used. Mice were housed 5 per

cage with a 12/12 h light/dark cycle (8:00 a.m. to 8:00 p.m.). Food and water were available *ad libitum*. After surgeries, mice were single housed to facilitate recovery. All experiments and behavioral study were performed during the light cycle (9:00 a.m. to 7:00 p.m.), and experimental protocol were in compliance with Zhejiang University Animal Experimentation and Ethics Committee and the ARRIVE guidelines (Percie du Sert et al., 2020). All efforts were made to minimize animal suffering and reduce the number of animals used.

Virus

For *in vivo* fiber photometry, Cre-inducible recombinant adeno-associated virus (AAV) vector containing GCaMP6s (*AAV-EF1a-DIO-GCaMP6s*, serotype: AAV2/9, viral titers: 2.05×10^{12} V.G./ml, 0.5 μl) was injected stereotactically into the PIL of *CR-cre* mice. For optogenetic modulation of CR neurons, 0.5 μl of *AAV-EF1a-DIO-hChR2(H134R)-EYFP* (serotype: AAV2/9, viral titers: 1.58×10^{13} V.G./ml) or *AAV-CAG-FLEX-ArchT-GFP* (serotype: AAV2/9, viral titers: 1.3×10^{13} V.G./ml) was injected stereotactically into the PIL of *CR-cre* mice. *AAV-Ef1α-DIO-eYFP* (serotype: AAV2/9, viral titers: 1.0×10^{13} V.G./ml, 0.5 μl) was used as control virus. *AAV2/2Retro-hEF1a-DIO-eYFP* (serotype: AAV2/2, viral titers: 1.73×10^{13} V.G./ml, 0.5 μl) and *AAV2/2Retro-hEF1a-DIO-mCherry* (serotype: AAV2/2, viral titers: 1.69×10^{13} V.G./ml, 0.5 μl) were injected stereotactically into the LA and ZI for retrograde tracing.

METHOD DETAILS

Stereotaxic surgery

Stereotaxic surgeries were performed according to our previous studies (Wang et al., 2016, 2017). Briefly, under sodium pentobarbital anesthesia (50 mg/kg, i.p.), mice were fixed onto a stereotaxic frame (512600, Stoelting) for virus injections and surgical implantations. Virus (0.5 μl) was injected into the PIL (AP: −3.1 mm; ML: −1.7 mm; DV: −3.6 mm) at a rate of 0.1 μl/min with a 1-μl microliter syringe controlled by pump (Micro4, World Precision Instruments). AAV viruses were allowed to express for at least 3 weeks before surgical implantation.

For *in vivo* fiber photometry and optogenetic modulation in hippocampal kindling model, electrodes made of twisted PFA-coated stainless-steel wires (791500; diameter, 0.127 mm; A-M Systems) were implanted into the right ventral hippocampus (CA3: AP: −2.9 mm; ML: −3.1 mm; DV: −3.0 mm) and affixed with dental cement for electrical stimulation and EEG recording. Then, an optical fiber attached to ceramic ferrule (200 μm, 0.37 NA, Inper Co. LTD) was implanted into the PIL and affixed with dental cement to deliver light. Two screws were placed over the cerebellum to serve as the reference and ground electrodes. For optogenetic modulation of PIL CR projections, the optic fiber was implanted into the LA (AP: −1.3 mm; ML: −3.2 mm, and DV: −3.0 mm) and ZI (AP: −1.8 mm; ML: −1.1 mm; DV: −4.3 mm) respectively.

In vivo fiber photometry

One week after surgery, fiber photometry was conducted during hippocampal kindling with the photometry system (Nanjing Thinkertech) according to our previous studies (Chen et al., 2020; Wang et al., 2020). Briefly, mice were placed in a dark room with an optic fiber connected to the PIL. Baseline GCaMP fluorescence was recorded for 100s followed by a 2-s kindling stimulation to the CA3 to elicit a hippocampal seizure, and then another 100s post stimulation was recorded. The GCaMP fluorescence was bandpass filtered and collected by a photomultiplier tube using a 488 nm diode laser that coupled into a 200 μm optical fiber. An amplifier was used to convert the current in the photomultiplier tube into voltage signals, which was further filtered through a low-pass filter (40 Hz). The data for the individual trial of kindling stimulations were analyzed and the values of fluorescence change ($\Delta F/F$) were derived by calculating $(F-F_0)/F_0$. F_0 is calculated by averaging the fluorescence signals of the 2 s prior to stimulation.

Kindling model

After one week of recovery from surgery, the CA3 of mice were stimulated with a constant-current stimulator (SEN-7203, SS-202J; Nihon Kohden) and the EEGs were recorded with a Neuroscan system (NuAmps, Neuroscan System). The stimulation intensity started at 40 μA and was increased by increments of 20 μA every 1 min until a 5 second after-discharge was produced. This stimulation intensity was defined as after-discharge threshold (ADT) of each mouse which indicated epileptogenic susceptibility. Mice with ADT that lower than 200 μA were used and grouped thereafter. Subsequently, all mice received 10 kindling stimulations daily (400 μA, 20 Hz, 2 s trains, 1 ms monophasic square-wave pulse) (Wang et al., 2020). The

seizure elicited by each stimulation was scored using a Racine's scale in which stage 1-3 are classified as FSs and stage 4-5 are classified as GSs (Racine, 1972). The seizure stages were systematically defined as stage 1: immobility; stage 2: nodding of head; stage 3: unilateral forelimb clonus; stage 4: rearing with bilateral fore-limb clonus; and stage 5: rearing with bilateral forelimb clonus followed by falling or spasmic jumping. Seizure stage was scored by a trained observer who was unaware of the experimental groupings.

Mice that exhibited 3 consecutive stage 5 seizures were defined as fully kindled. After mice were fully kindled, generalized seizure threshold (GST) was measured by giving stimulations starting at 80 μA and increased by increments of 40 μA until GS was achieved. To determine if modulation of CR neurons had an effect on GS, GST was used for stimulation and the stimulations were repeated for 9 times, initial 3 times for pre, next 3 times for light modulation and last 3 times for post. The generalized seizure duration (GSD) was calculated from the time that mice rearing with bilateral forelimb clonus to the end of after-discharge. Mice that experienced 3 consecutive stage 5 seizures were sacrificed for immunochemistry of c-Fos in GS (1.5h after last GS) according to the protocol of our prior research (Cheng et al., 2021).

Optogenetic modulation

The 473 nm (20 Hz, 10 ms/pulse, 5 mW) or 589 nm laser (continuous, 5 mW) was delivered by the laser (IKECOOL Laser) through a 200 μm optic fiber. The light stimulation was delivered immediately after kindling stimulation and lasted for 30 seconds.

Immunohistochemistry

Mice that had undergone behavioral test were anesthetized with pentobarbital (100 mg/kg, i.p.) and perfused transcardially with saline followed by 4% paraformaldehyde in 0.1M phosphate buffer. The brains were removed and postfixed in a solution of 4% phosphate-buffered paraformaldehyde at 4°C overnight. Then cryoprotect the brains with 30% (w/v) sucrose. The brains were sliced coronally to obtain 20 μm sections with cryostat (Thermos Scientific CryoStar NX70, USA). Brain sections were processed for immunofluorescence of CR (rabbit anti-CR, 1:1000, SWANT 7697), c-Fos (mouse anti-c-Fos, SANTA CRUZ, sc-166940), GAD (mouse anti-GAD65/67, 1:500 Millipore, AB1511), CaMKIIa (mouse anti-CaMKIIa, 1:400, Abcam ab32288), GFP (mouse anti-GFP, 1:500, Abcam ab10062) by incubating the sections with primary antibodies diluted with phosphate-buffered saline with 0.15% Triton X-100 overnight at 4°C, rinsed with phosphate-buffer saline, then incubated with donkey anti-mouse Alexa 488 or donkey anti-rabbit Alexa 594 conjugated fluorescent secondary antibody (715-545-150/711-585-152, Jackson Immuno Research Laboratories) 1 μg/ml for 2 h at room temperature. After incubation, the brain sections were once again washed and the immunofluorescence was assessed using a virtual slide microscope (Olympus VS120). Image J was used to tally CR neurons and cFos expression in each brain region. Three sections of each brain region were used for the average.

QUANTIFICATION AND STATISTICAL ANALYSIS

Data is expressed as means ± SEM. Number of experimental replicates (n) is indicated in each figure legend. Statistical comparisons were performed using Prism (version 9.0) with appropriate methods. Data were first tested by Kolmogorov-Smirnov test for normality and lognormality test, and data that do not exhibit a normal distribution were analyzed by non-parametric test. Data of seizure stage and ADD in kindling model were tested by two-way ANOVA followed by Dunnett's comparison test for multiple comparisons. Data of number of stimulations in each stage were tested by one-way ANOVA with Dunnett's multiple comparison test, or Kruskal-Wallis test with Dunn's multiple comparisons test. No statistical methods were used to pre-determine sample size. For all analyses, a two-tailed $p < 0.05$ was considered statistically significant. See details in Data S1.